Air Risk Maps for Unmanned Aircraft in Urban Environments

Air Risk Maps for Unmanned Aircraft in Urban Environments

Matteo Milano[1], Stefano Primatesta[1], Giorgio Guglieri[1]

***Abstract*— The increasing use of Unmanned Aircraft Systems (UAS) over inhabited areas requires the use of a suitable risk assessment. In this paper, we propose the use of air risk maps to assess the risk to people caused by mid-air collision accidents during a UAS flight operation.**

The proposed risk assessment tool is based on a state-of-the-art mathematical model for determining the rate of mid-air collisions of an unmanned aircraft with general aviation (GA). To evaluate the growing traffic of unmanned aircraft (UA), the model is also exploited to estimate the rate of mid-air collisions with other unmanned aircraft operating in the same airspace. The resulting rate of mid-air collisions is used to estimate the expected frequency of fatalities following mid-air collision accidents, here denoted as air risk. The air risk is computed using a probabilistic approach estimating the number of people involved in the accident, as well as the probability of fatality. Specifically, the air risk is computed for each geo-referenced element of the air risk map by combining several layers, including the population density and sheltering factor, as well as the physical parameters of the aircraft.

The proposed risk assessment tool is applied considering the Italian airspace, evaluating both the GA and UA traffic. Further analysis is also conducted to evaluate a future scenario with an increased number of UAS, observing a not negligible air risk.

I. Introduction

During the last decade, operations with lightweight Unmanned Aircraft Systems (UAS) have increased exponentially. The large diffusion of UAS is due to their flexibility and low cost, becoming a key element in the aviation field and producing a fast increment in the market. In the coming years, thanks to their rapid technological development, UAS will be widely used especially in cities [1], where UAS can be used to perform several applications within the Urban Air Mobility context [2]. However, the use of UAS over urban areas poses important challenges in public safety, privacy and cybersecurity [3].

For these reasons, National Aviation Authorities in most of the world countries strongly restrict the use of UAS in urban areas and, in any case, permitted under particular conditions, such as operating in a segregated airspace, with a limited MTOM (Maximum Take Off Mass) and, often, performed in VLOS (visual line-of-sight). In Europe, to perform a UAS flight operating in BVLOS (beyond visual line-of-sight) is often required to carry out the SORA (Specific Operations Risk Assessment) methodology [4], a risk assessment tool proposed by JARUS (Joint Authorities for Rulemaking of Unmanned Systems) and adopted by EASA (European Union Aviation Safety Agency). SORA is a multi-step process aiming at assessing the ground and air risk of a specific UAS operation, as well as determining necessary mitigations and robustness levels to guarantee an adequate level of safety. However, SORA is mainly a qualitative approach and, in critical and complex scenarios (e.g. urban areas) an additional and adequate risk analysis is required to enable the use of UAS [5].

In an our previous work [6], we have proposed the use of ground risk maps to estimate the ground risk of a specific UAS operation over large urban areas. The use of risk maps is a promising tool for risk-informed decision making able to quantify the ground risk of flying over urban areas, useful both for UAS operators and National Aviation Authorities to have an assessment of the risk distribution on urban areas. Moreover, as proposed in [7], [8], [9], the ground risk map can be also used to compute safe urban routes minimizing the overall ground risk and the flight time. However, the proposed risk assessment tool is able to assess only the ground risk. For the development of a complete tool of risk assessment the air risk must be evaluated.

The air risk assessed by SORA takes into account only the risk of mid-air collisions (MaC) with the manned aviation, neglecting the mid-air collisions with other unmanned aircraft. Nowadays, this assumption can be valid assuming a limited UAS traffic. However, considering an increase of UAS operations in the next years, the risk of mid-air collisions between unmanned aircraft should be taken into account.

Most of the studies about the estimation of the MaC rate are inherited from manned aviation dating back to the end of the 20th century, when the rise of General Aviation air traffic requires the evaluation of the MaC rate to guarantee an adequate level of safety [10], [11], [12]. A promising model have been proposed in [13], where an event-based approach is adopted, exploiting parameters that directly reflect physical properties of the aircraft flight, overcoming different shortcomings of the previous models [10], [11], [12]. Another important study is presented in [14], in which human and technical factors are relevant elements to be evaluated in the high-density airspace. Another step forward has been done in [15], including more detailed flight trajectories, time-dependent position errors, aircraft kinematics and wind.

Nevertheless, in the last years several studies have been performed considering the MaC rate of unmanned aircraft (UA). The importance of considering the MaC rate of UA is highlighted in [16], in which a collision risk model is developed and tested evaluating large-scale UA operations. Several approaches have been proposed to asses the risk of collision between GA and an UA. In [17], a model based on

[1]M. Milano, S. Primatesta and G. Guglieri are with the Department of Mechanical and Aerospace Engineering, Politecnico di Torino, Corso Duca degli Abruzzi 24, 10129 Torino, Italy. Corresponding author: Stefano Primatesta (e-mail: stefano.primatesta@polito.it)

the probability of collision between conflicting trajectories is proposed, while [18] exploits the use of Bayesian Networks. One of the most promising work has been introduced in [19], where the authors proposed a model for determining the MaC rate based on physical parameters of the aircraft and an estimation of the GA air traffic in a given airspace.

The aim of this work is the definition of air risk maps to quantify the air risk of UAS over large urban areas. The proposed air risk assessment tool estimates the MaC rate using the methodology proposed in [19]. Unlike [19], we use the mathematical model not only to estimate the MaC rate with the GA, but also with the UA air traffic. Then, the resulting MaC rate is used to assess the consequent risk to people on ground computing the expected rate of fatalities, here denoted as air risk. In fact, after a MaC occurs, the unmanned aircraft most likely loses control with the consequent impact on the ground and, then, risking to involve people. This severe consequence assumes great importance in densely populated areas. Furthermore, in this work, we also consider a future scenario by trying to estimate an increased UA traffic to demonstrate that the air risk will have a certain relevance, even in comparison with the ground risk.

The development of the air risk map, combined with the ground risk map proposed in [6], will offer an unprecedented tool for risk assessment for UAS over urban areas.

The paper is organized as follow. In Section II the concept of air risk map is introduced, while the model for the MaC rate estimation is described in Section III. Then, Section IV describes how parameters used for the computation of the MaC rate are defined. Results and analysis of the computed MaC rate, as well as an example of air risk map, are reported in Section V. Our conclusions are drawn in Section VI.

II. Risk Map

A. Ground Risk Map

Before introducing the air risk map proposed in this work, in this section we introduce the concept of ground risk map presented for the first time in [6], in which we have proposed the use of risk maps for the ground risk assessment for large urban areas. As defined in [6] a ground risk map is a two-dimensional location based map quantifying the risk to people on the ground for each cell in the map. The entire map is represented by a matrix of size N × M cells, that are equidistantly distributed and square shaped, and each of them represents a bounded geographical area. Each matrix element corresponds to a cell $R(i, j)$ containing a risk value, which is the risk for the associated geographical area. The discrete coordinates (i, j) represent a geo-referenced location (x, y) in the Local North-East-Down (NED) coordinate system defined with respect to the reference frame located in the center of the map.

Risk values are computed taking into account the risk level, no-fly zones and the presence of obstacles at the flight altitude. Practically, the ground risk map is obtained by merging several layers containing essential data required for the computation of the risk values. Such a layers have the same dimension and resolution of the ground risk map. As in [6], in this paper we evaluate the following layers:

- Population density layer: defines the population density and distribution in the map;
- Sheltering layer: defines the sheltering factor for each location in the map;
- Buildings layer: defines the height of buildings in the map;
- No-Fly zone layer: defines in which areas the flight is not permitted

Specifically, the Population density and Sheltering layers are used to compute the risk level of each element of the map, while Building and No-Fly zone layers define non-flyable areas.

In [6] the risk level corresponds with the ground risk assessed using a probabilistic risk assessment approach as in [20], [21], [17]. The ground risk is defined as the expected frequency of fatalities ($f^{\text{ground}}_{\text{fatality}}$) expressed in fatalities per flight hour (h^{-1}) and is computed as

$$f^{\text{ground}}_{\text{fatality}} = f_{\text{GIA}} \cdot N_{\text{impact}}(x, y) \cdot P_{\text{fatality}}(x, y), \quad (1)$$

with f_{GIA} is the rate that a ground impact accident occurs after an uncontrolled descent of the UAS. In [6] four descent event types are evaluated: ballistic descent, uncontrolled glide descent, parachute descent and the fly-away event. N_{impact} is the number of people exposed to the accident after the impact of the UAS on the ground. This value is affected by the population density and by the area exposed to the crash. P_{fatality} is the probability that the impacted people suffer of fatal injuries. This probability value depends on the kinetic energy at impact and on the so-called sheltering factor. By definition, the sheltering factor is a number greater than zero that quantifies the level of protection offered by objects like trees, buildings and cars to the people. In fact, the presence of objects in the impact area can reduce the kinetic energy at impact, reducing the probability to have a fatality. In particular, the frequency of fatalities $f^{\text{ground}}_{\text{fatality}}$ for each element of the map is computed evaluating the probabilistic impact area, aircraft parameters, environmental characteristics, as well as uncertainties on parameters. More details about the generation of the ground risk map are explained in [6].

B. Air Risk Map

The air risk map is a variation of the ground risk map, in which the risk level is associated with the air risk, instead of the ground risk. In particular, the air risk is defined as the expected frequency of fatalities ($f^{\text{air}}_{\text{fatality}}$) following MaC accidents [17]. Similarly to Equation (1), $f^{\text{air}}_{\text{fatality}}$ is computed as

$$f^{\text{air}}_{\text{fatality}} = f_{\text{MaC}} \cdot N_{\text{impact}}(x, y) \cdot P_{\text{fatality}}(x, y), \quad (2)$$

with f_{MaC} is the rate of MaC, N_{impact} and P_{fatality} are the number of people exposed to the consequent ground impact and the probability of fatality, respectively, and are defined as in Equation (1). Practically, we assume that, after a mid-air

collision, the UAS begins an uncontrolled descent with the consequent impact on the ground. Hence, the air risk level is computed using Equation (2) and using the same procedure of the ground risk map, i.e. using the multi-layer framework, evaluating the probabilistic impact area, aircraft parameters and environmental characteristics.

It is important to note that, in this work, we do not consider that the GA aircraft involved in the mid-air collision could also have catastrophic consequences. The study of the consequences of the impact between a UA and GA aircraft is not in the scope of this paper, even if a dedicated study is required to have a complete evaluation of the consequences of a mid-air collision between GA and UA.

The estimation of the f_{MaC} is performed using the methodology proposed in [19]. More details about the adopted methodology are explained in Section III.

III. Mid-Air Collision model

In this section we describe the methodology adopted to estimate the rate of Mid-air Collisions f_{MaC}. The methodology is based on the model developed in [19]. The model offers a rigorous mathematical approach in which general aviation aircraft (GA) and unmanned aircraft (UA) are represented as vertical cylinders considering the characteristic height *h* and radius *r* (i.e. the wingspan) of the aircraft.

This mathematical model is based on a series of simplifying assumptions: *(i)* UA and GA fly independently; *(ii)* within a predefined geographical area; *(iii)* at a flight altitude estimated by a probability density function f; *(iv)* with a flight direction uniformly distributed between $0°$ and $360°$; and *(v)* without moving along the vertical direction when near each other. The UA: *(vi)* always flies under a maximum allowed altitude $z_{\max}$; *(vii)* while the GA flies mostly over this altitude; *(viii)* even evaluating a probability that the GA aircraft flies below $z_{\max}$.

Based on these assumptions, as in [19], the MaC rate between a single GA aircraft and an UA is computed as

$$f_{\mathrm{MaC}} = p_{\mathrm{HC}} \cdot p_{\mathrm{VC}} \cdot p_{\mathrm{below}} \cdot \lambda_{\mathrm{STM}}, \tag{3}$$

with f_{MaC} is the rate of mid-air collisions, expressed as collisions per flight hours (h^{-1}). p_{HC} is the rate of horizontal collisions, i.e. when the two aircraft are in the same location in a NED reference system. p_{VC} is the conditional probability that the two aircraft fly at the same altitude and with null vertical velocity. Thus, this term depends on both the GA and UA altitude distribution functions. p_{below} quantifies the probability that the GA aircraft flies under the reference altitude $z_{\max}$, that is the maximum flight altitude at which the UA operates. This term depends on the GA altitude distribution function that changes based on the GA aircraft type considered. λ_{STM} is a mitigating factor which keeps into account the effect of tactical and strategic mitigations.

Equation (3) refers to the computation of the MaC rate between a single UA and a single GA. However, as introduced in [19], it can be expanded considering the expected GA inside the analyzed airspace as follow

$$f_{\mathrm{MaC}}^{\mathrm{tot}} = \sum_{i=1}^{\#\text{ of GA}} f_{\mathrm{MaC}}^{i} = \sum_{i=1}^{\#\text{ of GA}} p_{\mathrm{HC}}^{i} \cdot p_{\mathrm{VC}}^{i} \cdot n^{i} \cdot p_{\mathrm{below}}^{i} \cdot \lambda_{\mathrm{STM}}^{i}, \tag{4}$$

Practically, Equation (4) evaluates the rate f_{MaC} for each considered category of GA, which is characterized by the number of registered aircraft n, and, then, this rate is summed over the number of categories taken into account. As discussed in [19], it is possible to use this simplified formulation because of two important assumptions: *(i)* there aren't overlaps between the representative cylinders of different GA aircraft, that is acceptable considering the large dimensions of the analyzed airspace; *(ii)* because of the low value that f_{MaC} usually has, it is possible to not consider that, if the UA has a collision, it is unable to collide with other aircraft. More details about the mathematical model and about each term of Equations (3) and (4) are explained in [19].

The previously described methodology evaluates the MaC rate between GA traffic and a single UA. However, in this work the same approach is also used to evaluate the MaC rate between the UA air traffic and a single UA. In fact, in the next years the flight traffic of UA will increase exponentially and it is essential to evaluate also the UA air traffic data for a complete evaluation of the MaC rate. Specifically, the "external" UA aircraft involved in a possible collision is evaluated exactly as an additional GA aircraft type. Anyway, some different assumptions should be considered when the model parameters are defined, such as a probability equal to 1 that the "external" UA flies under the flight altitude $z_{\max}$.

IV. Model Parameter selection

Before generating the air risk map, several parameters about the GA and UA traffic, as well as the aircraft characteristics, have to be defined to estimate the MaC rate f_{MaC}. It is important to notify that the traffic data used to determine the parameters mentioned above refers to 2019, in order to avoid alterations due to the COVID-19 pandemic, and so, representing the real volume of traffic in the Italian airspace.

A. GA and UA traffic

In this work, five different categories of GA aircraft have been considered. Then, it has been possible to define a good representation of the Italian airspace. Specifically, we have considered the following categories, whose parameters are listed in Table I:

- **Fixed-wing aircraft**: this category includes fixed-wing aircraft equipped with a propulsive system, used for Air-Taxi operations, and aircraft with MTOM below 5700 kg, performing non-commercial operations;
- **Rotorcraft**: this category includes helicopters for commercial, non-commercial and specialized operations, with no limitations on the MTOM. HEMS (Helicopter

TABLE I

GA AND UA TRAFFIC PARAMETERS VALUES

	Fixed-wing	**Rotorcraft**	**Balloons**	**Gliders**	**HEMS**	**UA**
p_{below}	0.1%	5.0%	1.0%	10.0%	5.0%	100.0%
h [m]	2.0	3.0	25.0	1.2	3.9	0.29
r [m]	6.0	5.0	9.5	10.0	7.2	0.39
v [m/s]	75.0	56.0	10.0	50.0	75.4	13.6
n	13314	504	87	144	48	13566
T_{year} $[h^{-1}]$	100	147	17	32	200	21
f [m]	U(0, $z_{\max}$)	N(80, 50)	N(100, 60)	U(0, $z_{\max}$)	N(80, 50)	N(50, 30)

TABLE II

UA PARAMETERS VALUES

	Mavic Mini 2	**Hubsan Zino**	**Yuneec Typhoon H+**	**Parrot Disco Pro**	**Matrice 600 Pro**
h [m]	0.055	0.1	0.31	0.12	0.73
r [m]	0.1	0.16	0.26	0.575	0.84
v [m/s]	10.0	11.5	13.5	15.0	18.1
MTOM [kg]	0.25	0.7	1.99	0.94	15.5
f [m]	N(25, 20)	N(30, 25)	N(40, 25)	U(0, $z_{\max}$)	N(60, 40)

Emergency Medical Service) are excluded from this category;

- **Balloons**: comprehends the so-called "lighter-than-air" aircraft, which exploit hot air or other lighter-than-air gases for the flight;
- **Gliders**: group of fixed wing aircraft without propulsive system which take advance of the air currents;
- **Helicopter Emergency Medical Service (HEMS)**: air-rescue rotorcraft are considered in this category.

Parameters of Table I refer to the method presented in [19]. However, a brief description is reported for clarity: h and r are the height and radius of the aircraft cylinder; v is the average speed of the aircraft; n is the number of the GA (and UA) aircraft type in the considered area, i.e. the Italian airspace in this work; T_{year} is the flight hours per year; f is the altitude distribution below $z_{\max}$ defined with a uniform (U) or normal (N) distribution.

The number of aircraft registered in Italy for every single category has been estimated starting from the data included in [22], while the parameter T_{year} has been defined mainly referring to [23], but also evaluating the values used in [19] and reported in [24]. Despite [24] refers to the US airspace, a different airspace compared with the Italian one in terms of air traffic volume, it was useful, after an appropriate scaling, to have an initial estimation of the term T_{year}. Due to a lack of data, p_{below} is defined as in [19]. Regarding the distribution of the flight altitude, an estimation has been performed trying to have good representation of the behavior of each GA category under $z_{\max}$.

As mentioned in Section III, in this paper we also take into consideration the UA traffic in the computation of the MaC rate. Similarly to what has been done for the other GA categories, parameters of the UA traffic are also reported in Table I.

As previously discussed, we assume that the UA traffic is always below $z_{\max}$ and, then, p_{below} is defined equal to the 100%, as imposed by the regulatory framework. The physical characteristics of the "external" UA, such as dimensions and velocity, have been defined using the average values of the UAS reported in Table II. The motivation for this consideration is given by the fact that these UAS represent the different classes identified by EASA (C0, C1, C2 and C3) [4] and, then, representing UAS in the Italian airspace. Probably, this assumption does not reflect the real case, but it is a good compromise in order to demonstrate the validity of the proposed approach. The term n for the UA traffic is estimated using [22], in which all the UAS registered in Italy in 2019 are counted. Instead, the term T_{year} is defined evaluating the FAA survey [25]. The latter contains the flight habits of UAS pilots in the US, resulting in an average of seven monthly flights per each pilot with an average flight time of 15 minutes. Even if the survey in [25] refers to a different airspace, these data are useful for the purpose of the paper. The altitude distribution f has been defined evaluating an average distribution considering the UAS of Table II.

B. UAS parameters

In order to assess the air risk in different scenarios, five different models of unmanned aircraft have been chosen to perform the tests necessary to validate the model and analyze the influence of the different parameters. The different aircraft models are selected considering their different physical parameters, such as MTOM, dimensions, cruise velocity and, then, covering the different UAS categories identified by EASA (C0, C1, C2 and C3) [4]. The class C4 is not taken into account because, for the purposes of the paper, classes C3 and C4 have the same physical characteristics. Table II reports the parameters of the selected UA extracted from the data-sheets published by the manufacturers.

Most of the selected unmanned aircraft are multicopters, except a fixed-wing drone, selected to analyse how the MaC rate and, then, the air risk changes with this configuration, which involves a greater cruise velocity and a different altitude distribution function.

TABLE III

DATA USED TO COMPUTE THE AVG. EU MAC RATE

Total Occurrences (2019) [26]	941
French MaC ratio (2015-19) [27]	1%
Italian MaC ratio (2015-19) [28]	6.45%
Irish MaC ratio (2015-19) [29]	6.25%
Slovak MaC ratio (2016-19- [29]	2.9%
Romanian MaC ratio (2012-19) [31]	4.4%
Average EU MaC ratio	4.2%
Total MaC (2019)	40
Total Flights (2019) [32]	11 105 855
Average EU MaC rate (2019)	$3.56 \cdot 10^{-6}$ h^{-1}

C. Average European MAC rate

In order to evaluate the obtained MaC rates, it is necessary to determine some reference values of f_{MaC}.

First, we have tried to define an average European MaC rate. Using data reported in [26], it has been possible to calculate the total number of air accidents, in which aircraft of the considered categories have been involved during 2019 inside the European airspace. Then, analysing several European Safety Reports, related to the period 2015-2019 published by France [27], Italy [28], Ireland [29], Slovakia [30] and Romania [31], it has been possible to evaluate the ratio of collision events compared to the total number of flights in the National airspace, for each one of the above mentioned Countries. Thus, an average ratio of collision events is estimated for the European airspace. Finally, using the total number of flight hours in the European airspace during 2019, extracted from [32], it has been possible to estimate the average European MaC rate, expressed as collisions per flight hours (h^{-1}). Table III shows the key values previously discussed.

According to what is reported in the ICAO Annex 13 [33], three categories of air accidents are taken into account in the Safety Reports: accident, serious incident and incident. Then, the computed European MaC rate is overestimated since it evaluates also air accidents not considered by the adopted model. On the contrary, the European MaC rate has been calculated on the basis of scarce data, which represent only a portion of the EU member States.

For comparison, we also use the value of $1 \cdot 10^{-7}\mathrm{h}^{-1}$ on each plot about the MaC rate, that is, according with [19], [17], the order of magnitude of the Equivalent Level Of Safety (ELOS) for GA. Instead, the ELOS threshold used for the air risk is $1 \cdot 10^{-6}\mathrm{h}^{-1}$, as discussed in [17], [6].

V. RESULTS

A. Implementation

The methodology for the computation of air risk maps is implemented in C++ as an executable process in the ROS (Robot Operating System) framework [34].

The software is developed to be compatible with the ground risk map proposed in [6] in order to have a complete risk assessment tool able to evaluate both the ground and air risk over large areas. For this reason, the multilayer framework is generated using Grid Map [35], a ROS-based C++ library able to manage two-dimensional grid maps with multiple data layers.

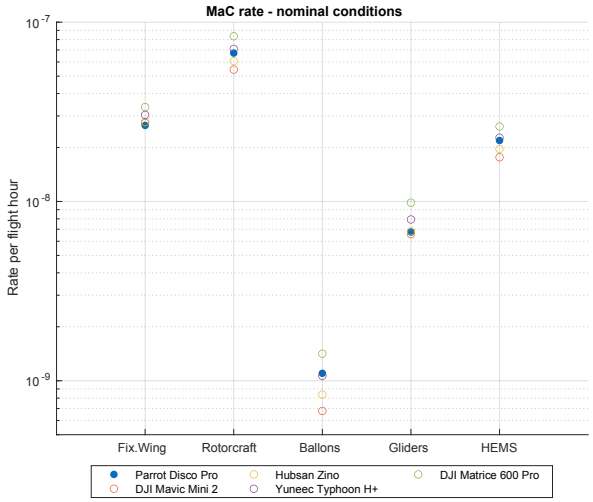

Figure 1. The MaC rate with nominal conditions and without the UA traffic for each GA category and for each UA of Table II.

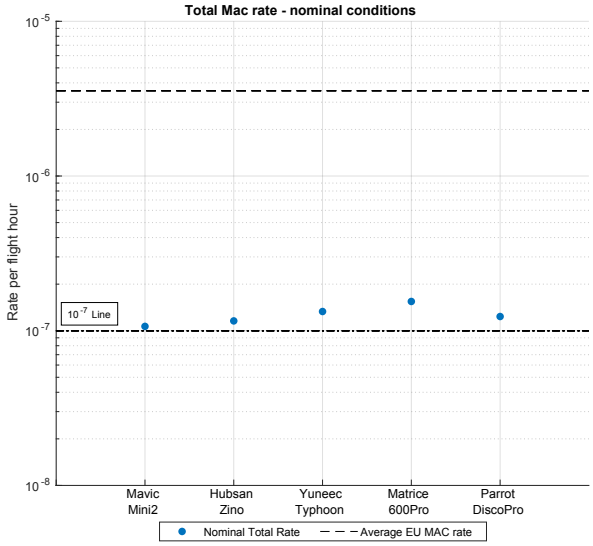

Figure 2. The total MaC rate with nominal conditions and without the UA traffic computed for each UA of Table II.

B. Mid-air Collision Rate Analysis

We have conducted some preliminary analyses about the MaC rate computed. This analysis aims to identify the effect of the different parameters, as well as how the MaC rate changes with different traffic conditions. It should be noted that in these tests we neglected the mitigation factor defining $\lambda_{\mathrm{STM}} = 1$.

Nominal Conditions: First, we have computed the MaC rate using the nominal GA traffic conditions of Table I without considering the UA air traffic and with $z_{\max} = 120$ m, i.e. the maximum flight altitude permitted by EASA for typical UAS operations. As shown in Figure 1, we have computed the MaC rate for each considered drone in respect to every single category of GA. Analysing Figure 1, as

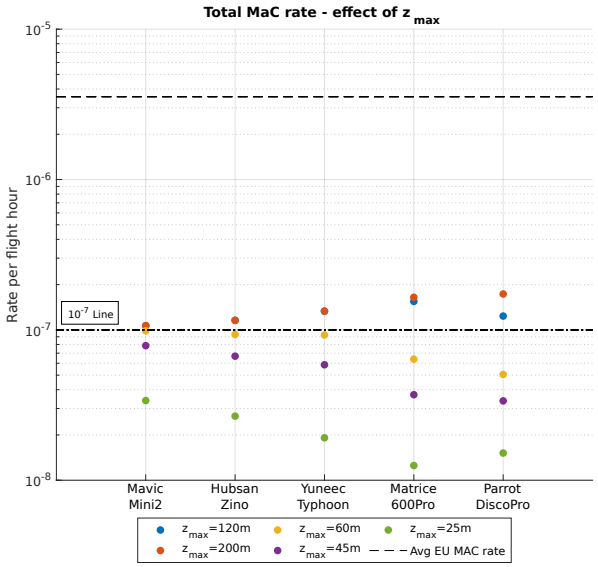

Figure 3. The MaC rate computed using different values of $z_{\max}$. The MaC rate is computed at the nominal conditions and without the UA traffic.

expected, the MaC rate depends on the different dimensions assumed for the GA aircraft and the number of aircraft belonging to a specific GA category. Furthermore, also the drone dimensions affect the MaC rate, and, then, slightly increasing from the DJI Mavic Mini 2 (C0) to the DJI Matrice 600 Pro (C3).

The effect of the drone dimensions and velocity can also be observed in Figure 2, which shows the total MaC rate $f_{\text{MaC}}^{\text{tot}}$ of each UA considered. It is clearly visible that for each UA the total MaC rate is on the order of $1 \cdot 10^{-7}$ h^{-1}, below the average European MaC rate and comparable with the ELOS for GA.

Effect of $z_{\max}$: Another interesting analysis involves the effect of the maximum flight altitude $z_{\max}$ on the estimated MaC rate. In the previous tests we have defined $z_{\max} = 120$ m, that is the maximum flight altitude admissible by EASA for typical UAS operations. However, often, unmanned aircraft do not operate at this altitude and, then, it is useful to evaluate how the flight altitude affects the MaC rate. The effect of $z_{\max}$ is shown in Figure 3.

As expected, with a lower value of $z_{\max}$, the MaC rate decreases, and, this is emphasized with UA with bigger dimensions and higher velocity. This trend is due to the reduction of p_{VC}, which depends on the altitude distribution function of both UA and GA. Then, lowering the maximum allowable altitude, the probability of being at the same flight altitude of the GA is reduced, decreasing the resulting MaC rate f_{MaC}. On the contrary, increasing $z_{\max}$ to 200 m, the resulting MaC rate grows as expected. This is more visible with the Parrot Disco Pro and with the Matrice 600 Pro due to their flight distributions. With the other UA, the effect is not relevant because of their altitude distribution functions that are definitely lower than $z_{\max}$. It should be noted that, in this test, to highlight the effect of $z_{\max}$, the value of p_{below} is not modified.

TABLE IV
PARAMETERS USED TO INCREMENT THE GA TRAFFIC

Increment	n	T_{year} $[h^{-1}]$
2x	2x	+20%
3x	3x	+30%
5x	5x	+50%

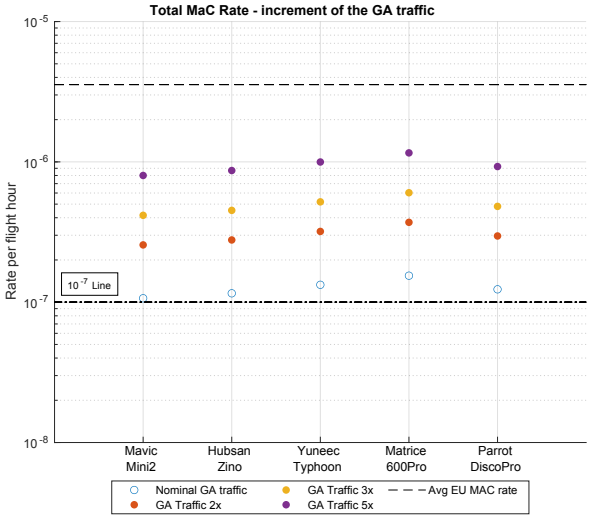

Figure 4. The resulting MaC rate considering an increment of the GA air traffic, as reported in Table IV.

Effect of the GA traffic volume: Despite the effects of the COVID-19 pandemic, aviation is a rapidly growing sector, and, for this reason, it is realistic to assume an increase in the GA air traffic volume. To evaluate the relation between the GA traffic growth and the collision rate, we have increased the parameters *n* and *T*, as reported in Table IV. We do not have equally increase *n* and *T* because, even if the number of aircraft rises, the habits of pilots may not increase as well, limiting the increase in the airspace occupation time.

Observing Figure 4, we can note that, as expected, the MaC rate increases with the GA traffic for all the categories of UA, highlighting how the effect of the parameters *n* and *T* is relevant. Furthermore, it is possible to notice that for an increment of 5x of the GA traffic, the resulting f_{MaC} is about $1 \cdot 10^{-6}$ h^{-1}, an order of magnitude greater than the ELOS for GA ($1 \cdot 10^{-7}$ h^{-1}).

Effect of the UA traffic volume: As previously stated, one of the main objectives of this work is to evaluate the influence of the presence of UA traffic on the air risk.

Figure 5 shows the effect of the nominal UA traffic of Table I on the nominal GA traffic condition and using $z_{\max} = 120$ m. It is possible to observe that when UA traffic is considered, the resulting MaC rate is almost doubled, especially for larger drones like the DJI Matrice 600 Pro.

Furthermore, Figure 6 reports the results considering an increasing of the UA traffic. The UA traffic volume is increased using the parameters reported in Table V. Observing Figure 6, we can see that, as expected, the resulting MaC rate increases a lot with the increased UA traffic. In particular, with the bigger UA, i.e. the DJI Matrice 600, the order of

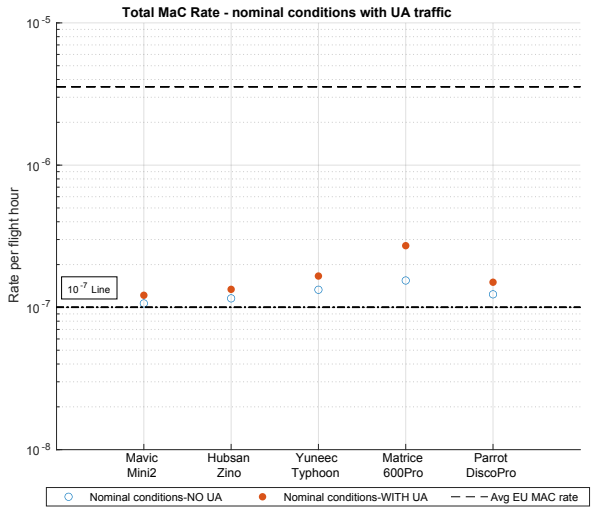

Figure 5. Total MaC rate considering the nominal conditions with the UA air traffic.

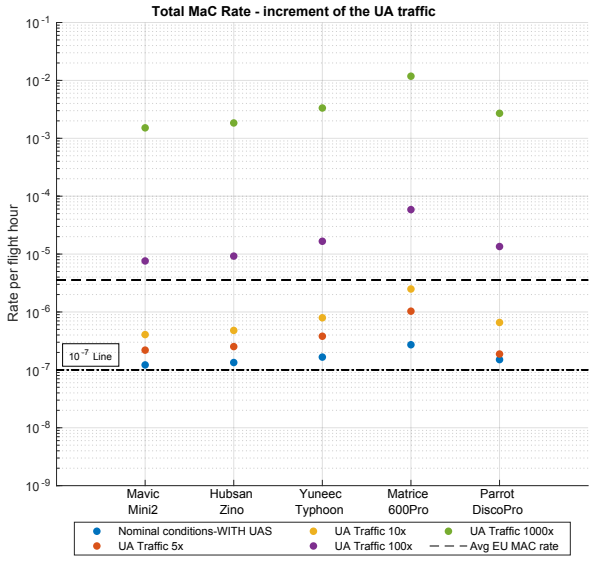

Figure 6. Total MaC rate considering an increased UA traffic volume.

TABLE V
PARAMETERS USED TO INCREMENT THE UA TRAFFIC

Increment	n	$T_{\text{year}}[h^{-1}]$
5x	5x	+50%
10x	10x	+100%
100x	100x	+1000%
1000x	1000x	+10000%

magnitude of $1 \cdot 10^{-6}$ h^{-1} is reached with an increase of 5x of the UA traffic, that is a realistic scenario in the next few years. Obviously, the MaC rate is much higher with a UA traffic increased of 100x and 1000x.

C. Air Risk Map Analysis

In this section we report and discuss the resulting air risk map generated using Equation (2) and the MaC rate previously discussed.

As mentioned in Section II, the air risk map is constructed using the same procedure of the ground risk map introduced in [6]. The only main difference is the computation of the risk level for each element of the map that is computed using the air risk assessment of Equation (2).

In order to test the air risk map, we have selected an urban area of the city center of Turin, Italy, that is a critical operative area for the use of drones. The selected area is shown in Figure 7(a).

The air risk map is constructed using the Population Density and Sheltering Factor layers shown in Figures 7(b) and 7(c), respectively. These layers are generated as discussed in [6]. The Population Density layer is based on a realistic database of the population density and distribution in Turin, Italy. The Sheltering Factor layer is defined using OpenStreetMap, in which a sheltering level equal to 8 is associated to a map element occupied by buildings, while a sheltering level of 3 to all other elements.

Using these layers, we have generated the air risk pap of Figure 8(a) evaluating the DJI Matrice 600 Pro. The MaC rate is computed considering the nominal GA and UA traffic of Table I. Instead, the number of involved people and the probability of fatality are computed using the same method adopted in [6].

In order to analyse the resulting risk, we have compared the air risk map with the ground risk map presented in [6]. The resulting ground risk map is illustrated in Figure 8(b) and it is computed using a rate of ground impact accident of $f_{\text{GIA}} = 1/200$ h^{-1}, while N_{impact} and P_{fatality} are computed as in the air risk map.

Comparing Figures 8(a) and 8(b), we can observe that the distribution of the risk on the map is the same. This happens because Equations (2) and (1) differ in the term f_{MaC} and f_{GIA}, respectively. In both air and ground risk maps, the risk is higher in areas with a higher population density and with a lower sheltering factor. Instead, comparing the minimum, maximum and average risk reported in Table VI, we can affirm that the air risk is irrelevant compared with the ground risk.

Our hypothesis is defined evaluating the nominal GA and UA air traffic. Anyway, the operational scenario will be completely different in a few years. Although in a simplified way, we tried to evaluate a future scenario increasing the UA traffic and, on the contrary, decreasing the rate of ground impact accidents. In fact, we assume that in the next future the UA traffic will increase exponentially but, on the contrary, the reliability of unmanned aircraft will be improved. Tables VI and VII report the risk values considering the DJI Matrice 600 Pro and the DJI Mini 2, respectively, and assuming an increasing of the UA air traffic. As expected, these assumptions increase the resulting air risk and, on the opposite, decrease the ground risk.

Analyzing the risk levels of Tables VI and VII, the air risk and the ground risk are comparable in the scenario with the UA traffic increased of 100x, while the air risk is greater than the ground risk in the scenario with the UA traffic increased of 1000x. Even if this is a future scenario, it will

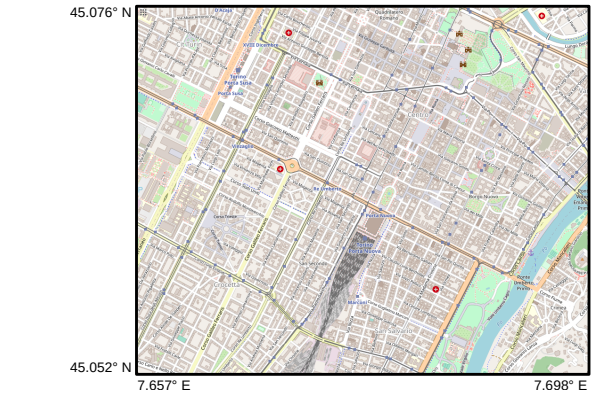

(a)

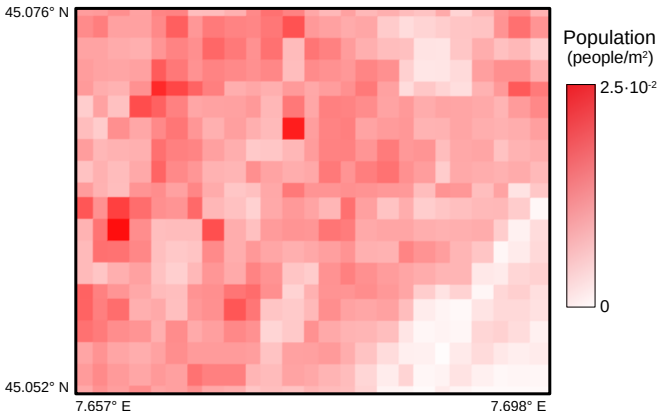

(b)

(c)

Figure 7. From top to bottom: in (a) the area from OpenStreetMap used to generate the air risk map; in (b) the Population Density layer; and in (c) the Sheltering Factor layer.

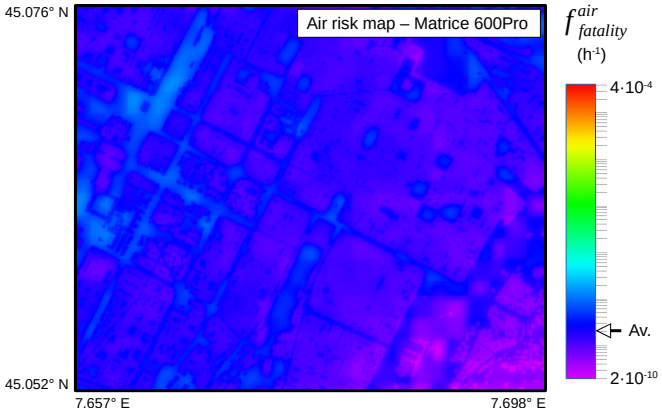

(a)

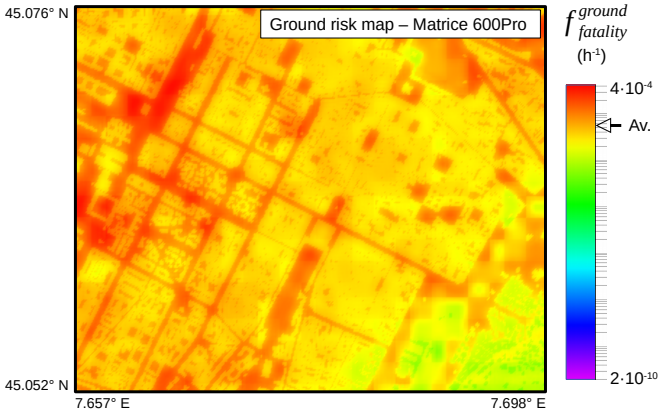

(b)

Figure 8. In (a) the air risk map, while in (b) the ground risk map. Both maps are computed evaluating the DJI Matrice 600 Pro.

be essential to consider air risk mitigations with increasing of UA traffic. In fact, mitigations reduce the MaC rate and, as a consequence, also the air risk.

Moreover, in case of heavy unmanned aircraft, such as the DJI Matrice 600 Pro, the air risk assumes values greater than the ELOS for UA ($1 \cdot 10^{-6}$ h^{-1}) in the scenario with the UA traffic increased of 100x and 1000x.

VI. Conclusions

In this work we have proposed the use of air risk maps to quantify the air risk over large urban areas. The proposed approach estimates the Mid-air Collision rate of an unmanned aircraft with the General Aviation and Unmanned Aircraft traffic. The MaC rate is computed using the approach proposed in [19] and applied also evaluating the UA traffic. The estimated MaC rate is then used to compute the resulting risk to people on ground generating the so-called air risk map.

We have also conducted several analysis about the MaC rate evaluating how it changes using several unmanned aircraft model and considering several scenarios with an increased air traffic volume. Considering the current GA and UA traffic data, the resulting MaC rate is about $1 \cdot 10^{-7}$ h^{-1}, a value comparable with the Equivalent Level Of Safety for

TABLE VI

AIR AND GROUND RISK VALUES WITH THE DJI MATRICE 600 PRO AIRCRAFT.

UA traffic	f_{MaC} [h^{-1}]	f_{GIA} [h^{-1}]		$f^{\mathrm{air}}_{\mathrm{fatality}}$ [h^{-1}]	$f^{\mathrm{ground}}_{\mathrm{fatality}}$ [h^{-1}]
1x	$2.67 \cdot 10^{-7}$	$1/200$	min	$2.06 \cdot 10^{-10}$	$3.86 \cdot 10^{-6}$
			max	$1.83 \cdot 10^{-8}$	$3.43 \cdot 10^{-4}$
			av	$2.86 \cdot 10^{-9}$	$5.35 \cdot 10^{-5}$
5x	$1.14 \cdot 10^{-6}$	$1/1000$	min	$8.81 \cdot 10^{-10}$	$7.73 \cdot 10^{-7}$
			max	$7.82 \cdot 10^{-8}$	$6.86 \cdot 10^{-5}$
			av	$1.22 \cdot 10^{-8}$	$1.07 \cdot 10^{-5}$
10x	$2.54 \cdot 10^{-6}$	$1/2000$	min	$1.96 \cdot 10^{-9}$	$3.86 \cdot 10^{-7}$
			max	$1.74 \cdot 10^{-7}$	$3.43 \cdot 10^{-5}$
			av	$2.72 \cdot 10^{-8}$	$5.35 \cdot 10^{-6}$
100x	$6.08 \cdot 10^{-5}$	$1/10000$	min	$4.70 \cdot 10^{-8}$	$7.73 \cdot 10^{-8}$
			max	$4.17 \cdot 10^{-6}$	$6.86 \cdot 10^{-6}$
			av	$6.50 \cdot 10^{-7}$	$1.07 \cdot 10^{-6}$
1000x	$1.21 \cdot 10^{-2}$	$1/10000$	min	$9.35 \cdot 10^{-6}$	$7.73 \cdot 10^{-8}$
			max	$8.30 \cdot 10^{-4}$	$6.86 \cdot 10^{-6}$
			av	$1.29 \cdot 10^{-4}$	$1.07 \cdot 10^{-6}$

TABLE VII

AIR AND GROUND RISK VALUES WITH THE DJI MAVIC MINI 2 AIRCRAFT.

UA traffic	f_{MaC} [h^{-1}]	f_{GIA} [h^{-1}]		$f^{\mathrm{air}}_{\mathrm{fatality}}$ [h^{-1}]	$f^{\mathrm{ground}}_{\mathrm{fatality}}$ [h^{-1}]
1x	$1.24 \cdot 10^{-7}$	$1/200$	min	$5.59 \cdot 10^{-14}$	$2.26 \cdot 10^{-9}$
			max	$6.07 \cdot 10^{-12}$	$2.45 \cdot 10^{-7}$
			av	$1.24 \cdot 10^{-12}$	$5.01 \cdot 10^{-8}$
5x	$2.18 \cdot 10^{-7}$	$1/1000$	min	$9.83 \cdot 10^{-14}$	$4.51 \cdot 10^{-10}$
			max	$1.07 \cdot 10^{-11}$	$4.89 \cdot 10^{-8}$
			av	$2.18 \cdot 10^{-12}$	$1.00 \cdot 10^{-8}$
10x	$4.01 \cdot 10^{-7}$	$1/2000$	min	$1.81 \cdot 10^{-13}$	$2.26 \cdot 10^{-10}$
			max	$1.96 \cdot 10^{-11}$	$2.45 \cdot 10^{-8}$
			av	$4.02 \cdot 10^{-12}$	$5.01 \cdot 10^{-9}$
100x	$7.96 \cdot 10^{-6}$	$1/10000$	min	$3.59 \cdot 10^{-12}$	$4.51 \cdot 10^{-11}$
			max	$3.90 \cdot 10^{-10}$	$4.89 \cdot 10^{-9}$
			av	$7.97 \cdot 10^{-11}$	$1.01 \cdot 10^{-9}$
1000x	$1.64 \cdot 10^{-3}$	$1/10000$	min	$7.40 \cdot 10^{-10}$	$4.51 \cdot 10^{-11}$
			max	$8.03 \cdot 10^{-8}$	$4.89 \cdot 10^{-9}$
			av	$1.64 \cdot 10^{-8}$	$1.01 \cdot 10^{-9}$

GA [17], [19].

Furthermore, we have compared the proposed air risk map with the ground risk map presented in our previous work [6]. As result, the air risk maps include an air risk that is irrelevant compared with the ground risk. However, in case of UA traffic increased of 100x and 1000x, the resulting air risk is not negligible. Even if these scenarios are unrealistic in the next few years, the effect of 100x and 1000x traffic should be considered for the update of the current regulatory framework. In fact, our analysis suggests that in a future scenario the use of air risk mitigations, both tactical and strategic are required.

Results are based on assumptions and considerations made to the best of the knowledge of the authors. In fact, the scope of the paper is to define a method for air risk assessment. Hence, a further analysis of the air traffic data may be necessary to analyze a more realistic scenario.

The proposed air risk map, combined with the ground risk map proposed in [6], is a promising tool for risk assessment. It can be used either by UAS operators and National Aviation Authorities to quantify the risk of a specific UAS operation, as well as to plan a safe route in urban areas, as in [8], [7], [9].

Future works will include the evaluation of a more detailed UA traffic, analysing each UAS category (C0, C1, C2, C3 and C4) independently. Moreover, the mitigation factor can be estimated and used to produce more realistic results.

REFERENCES

[1] N. Bloise, S. Primatesta, R. Antonini, G. P. Fici, M. Gaspardone, G. Guglieri, and A. Rizzo, "A survey of unmanned aircraft system technologies to enable safe operations in urban areas," in *2019 International Conference on Unmanned Aircraft Systems (ICUAS)*. IEEE, 2019, pp. 433–442.

[2] A. Straubinger, R. Rothfeld, M. Shamiyeh, K.-D. Büchter, J. Kaiser, and K. O. Plötner, "An overview of current research and developments in urban air mobility–setting the scene for uam introduction," *Journal of Air Transport Management*, vol. 87, p. 101852, 2020.

[3] E. Vattapparamban, I. Güvenç, A. I. Yurekli, K. Akkaya, and S. Uluağaç, "Drones for smart cities: Issues in cybersecurity, privacy, and public safety," in *2016 international wireless communications and mobile computing conference (IWCMC)*. IEEE, 2016, pp. 216–221.

[4] E. U. A. S. Agency, "Easy access rules for unmanned aircraft systems (regulations (eu) 2019/947 and (eu) 2019/945)," 2021.

[5] P. S. ECA, "Specific operations risk assessment (SORA) – ECA position paper," 2021.

[6] S. Primatesta, A. Rizzo, and A. la Cour-Harbo, "Ground risk map for unmanned aircraft in urban environments," *Journal of Intelligent & Robotic Systems*, vol. 97, no. 3, pp. 489–509, 2020.

[7] S. Primatesta, G. Guglieri, and A. Rizzo, "A risk-aware path planning strategy for uavs in urban environments," *Journal of Intelligent & Robotic Systems*, vol. 95, no. 2, pp. 629–643, 2019.

[8] S. Primatesta, L. S. Cuomo, G. Guglieri, and A. Rizzo, "An innovative algorithm to estimate risk optimum path for unmanned aerial vehicles in urban environments," *Transportation research procedia*, vol. 35, pp. 44–53, 2018.

[9] S. Primatesta, M. Scanavino, G. Guglieri, and A. Rizzo, "A risk-based path planning strategy to compute optimum risk path for unmanned aircraft systems over populated areas," in *2020 International Conference on Unmanned Aircraft Systems (ICUAS)*. IEEE, 2020, pp. 641–650.

[10] S. Endoh, "Aircraft collision models," Ph.D. dissertation, Massachusetts Institute of Technology, 1982.

[11] J. M. Richie, "Description of the derivation of the collision risk model used in the vertical separation simulation risk model," Federal Aviation Administration Technical Center Atlantic City, Tech. Rep., 1989.

[12] K. Datta and R. Oliver, "Predicting risk of near midair collisions in controlled airspace," *Transportation Research Part B: Methodological*, vol. 25, no. 4, pp. 237–252, 1991.

[13] P. Brooker, "Lateral collision risk in air traffic track systems: a 'post-reich'event model," *The Journal of Navigation*, vol. 56, no. 3, pp. 399–409, 2003.

[14] H. Blom, B. Bakker, M. Everdij, and M. Van Der Park, "Collision risk modeling of air traffic," in *2003 European Control Conference (ECC)*. IEEE, 2003, pp. 2236–2241.

[15] M. Fujita, "Collision risk model for independently operated homogeneous air traffic flows in terminal area," *Electronic Navigation Research Institute Papers*, no. 130, 2013.

[16] D. Janisch, P. Sánchez-Escalonilla, V. Gordo, and M. Jiménez, "Uav collision risk as part of u-space demand and capacity balancing."

[17] K. Dalamagkidis, K. P. Valavanis, and L. A. Piegl, *On integrating unmanned aircraft systems into the national airspace system: issues, challenges, operational restrictions, certification, and recommendations*. Springer, 2009.

[18] J. A. V. C. H. Usach Molina, "Automated contingency management in unmanned aircraft systems," Ph.D. dissertation, Universitat Politècnica de València, 2019.

[19] A. la Cour-Harbo and H. Schiøler, "Probability of low-altitude midair collision between general aviation and unmanned aircraft," *Risk Analysis*, vol. 39, no. 11, pp. 2499–2513, 2019.

[20] R. Clothier, R. Walker, N. Fulton, and D. Campbell, "A casualty risk analysis for unmanned aerial system (UAS) operations over inhabited areas," in *Proceedings of AIAC12: 2nd Australasian Unmanned Air Vehicles Conference*. Bristol UAV Conference, 2007, pp. 1–16.

[21] A. la Cour-Harbo, "Quantifying risk of ground impact fatalities for small unmanned aircraft," *Journal of Intelligent & Robotic Systems*, vol. 93, no. 1, pp. 367–384, 2019.

[22] GAMA, "Databook 2019," Available at: https://gama.aero/wp-content/uploads/GAMA_2019Databook_Final-2020-03-20.pdf, General Aviation Manufacturers Association, Tech. Rep., 2020.

[23] ENAC, "Dati traffico 2019," Available at: https://www.sipotra.it/wp-content/uploads/2020/07/Dati-di-traffico-2019.pdf, Ente Nazionale Aviazione Civile, Tech. Rep., 2020.

[24] FAA, "General aviation and part 135 activity survey," Available at: https://www.faa.gov/data_research/aviation_data_statistics/general_aviation/CY2019/, Federal Aviation Agency, Tech. Rep., 2020.

[25] ——, "Aerospace forecast fiscal years 2021-2041," Available at: https://www.faa.gov/data_research/aviation/aerospace_forecasts/media/Unmanned_Aircraft_Systems.pdf, Federal Aviation Agency, Tech. Rep., 2021.

[26] EASA, "Annual safety review 2020," Available at: https://www.easa.europa.eu/sites/default/files/dfu/easa_asr_2020.pdf, European Aviation Safety Agency, Tech. Rep., 2021.

[27] MEEM, "Rapport sur la securite aerienne 2015 - 2019," Ministère de l'environnement de l'energie et de la mer, Tech. Rep., 2016 - 2020.

[28] ENAC, "Safety report: Safety data 2015-2019," Ente Nazionale Aviazione Civile, Tech. Rep., 2020.

[29] IAA, "Review of aviation safety performance in ireland: during 2015-2019," Irish Aviation Authority, Tech. Rep., 2016 - 2020.

[30] SCAA, "Povzetek letnega poročila o letalski varnosti 2016 - annual aviation safety review 2016 - 2019," Slovak Civil Aviation Agency, Tech. Rep., 2017 - 2020.

[31] RCAA, "Informare anuală de siguranţă 2012-2019 - safety review 2012-2019," Romanian Civil Aviation Authority, Tech. Rep., 2020.

[32] EUROCONTROL, "Network operations report 2019," Available at: https://www.eurocontrol.int/sites/default/files/2020-04/nm-annual-network-operations-report-2019-main-report.pdf, Tech. Rep., 2020.

[33] ICAO, "Annex 13: Aircraft accident and incident investigation," 2020.

[34] M. Quigley, K. Conley, B. Gerkey, J. Faust, T. Foote, J. Leibs, R. Wheeler, A. Y. Ng *et al.*, "Ros: an open-source robot operating system," in *ICRA workshop on open source software*, vol. 3, no. 3.2. Kobe, Japan, 2009, p. 5.

[35] P. Fankhauser and M. Hutter, "A universal grid map library: Implementation and use case for rough terrain navigation," in *Robot Operating System (ROS)*. Springer, 2016, pp. 99–120.